Available online at www.sciencedirect.com
ScienceDirect
BioSystems 89 (2007) 101–109
Bio Systems
www.elsevier.com/locate/biosystems

Modelling the early steps of transduction in insect olfactory receptor neurons

Jean-Pierre Rospars [a,*], Philippe Lucas [a], Mathieu Coppey [a,b]

[a] *UMR1272 UPMC–INRA–INA-PG "Physiologie de l'insecte", INRA, 78026 Versailles Cedex, France*
[b] *Laboratoire de Physique Théorique des Liquides, Université Pierre et Marie Curie (UPMC), 75252 Paris Cedex 05, France*

Received 24 November 2005; accepted 22 May 2006

Abstract

Olfactory transduction is a multistep process whose basic function is to convert a low energy reaction, the odorant-receptor interaction that may involve a single odorant molecule, into a whole cell electrical response, the receptor potential, which triggers the firing of one or more action potentials. Although much effort has been devoted to the experimental analysis of transduction in olfactory receptor neurons (ORNS), especially in the favorable moth sex-pheromone receptor neuron, its modelling is less advanced. The model we investigated, which takes into account the translocation of pheromone molecules from air to the extracellular space, their deactivation and their interaction with receptors, focuses on the membrane cascade. It involves the interaction of receptors, G-proteins and effector enzymes, whose reaction rates are limited by lateral diffusion in the membrane. The evolutions in time of these species in response to single pulse stimulation of various intensities were compared to one another and to the experimentally measured electrical response. The results obtained suggest that the receptor-to-effector conversion is fast with respect to the receptor response, that it presents a small amplification factor, contrary to the photoreceptor, and that most of the amplification is achieved in the post-effector processes involving the second messenger and ionic channels.

Keywords: Olfaction; Neuron model; Sexual pheromone; Transduction; Lateral diffusion

1. Introduction

Olfaction is involved in food and mate location, social interactions, and interspecific communication and is thus of major importance for the survival of most animal species. The olfactory systems have evolved to discriminate a large number of odor molecules. This discrimination is performed by several hundreds of odorant receptor proteins in vertebrates and several tens in insects, each olfactory receptor neuron (ORN) expressing a single type of odorant receptor (OR). This discovery (Buck and Axel, 1991) earned their authors the Nobel Prize in 2004. The reliance on the sense of smell is especially conspicuous in moths whose males can sense minute amounts of the sexual pheromone emitted by conspecific females. Usually a moth pheromone is a blend in a specific ratio of 2 to 3 hydrocarbon molecules with 12 to 16 carbon atoms. The male pheromone system is uniquely devoted to the detection of the pheromone. It is composed of several thousand neurons typically associated in pairs within specialized hair-like units, the sensilla, each neuron expressing one of the 2 or 3 pheromone receptor proteins. This specialization is a major difference with other olfactory subsystems for which a given olfactory receptor can respond to several

* Corresponding author. Tel.: +33 1 30 83 33 55; fax: +33 1 30 83 31 19.
E-mail address: rospars@versailles.inra.fr (J.-P. Rospars).

0303-2647/$ – see front matter © 2006 Elsevier Ireland Ltd. All rights reserved.
doi:10.1016/j.biosystems.2006.05.015

(usually unknown) related odorant molecules. The fact that the ligands of receptors are known and the sensilla can be morphologically recognized and individually recorded from, explain why the pheromone system is an excellent preparation for the experimental study of olfactory processes (see reviews by Stengl et al., 1999; Kaissling, 2004; Vogt, 2004; Jacquin-Joly and Merlin, 2004).

The pheromone molecules enter the hair lumen through multiple pores. In the sensillum lymph they are transported by pheromone binding proteins (PBP, Vogt and Riddiford, 1981) to the neuron membrane and metabolized by pheromone degrading enzymes (Kasang, 1971; Ishida and Leal, 2005). The pheromone receptor neuron is a typical ORN. Its outer dendritic membrane contains the transduction machinery, which yields a membrane depolarization in the presence of pheromone molecules. The early steps of transduction involve the sequential interaction of three types of proteins—pheromone receptors, G-proteins, and effector enzymes. The effector catalyzes the formation of second-messenger molecules open ion channels and depolarize the membrane, yielding the receptor potential. The pheromone receptor of the silkmoth *Bombyx mori* has recently been identified (Krieger et al., 2004; Nakagawa et al., 2005). The effector is phospholipase C (Breer et al., 1990; Maida et al., 2000) which catalyzes the cleavage of phosphatidylinositol biphosphate PIP_2 in inositol triphosphate IP_3 and diacylglycerol DAG, whose respective roles have not yet been completely clarified (Stengl, 1994; Zufall and Hatt, 1991; Pophof and van der Goes van Nanters, 2002; Pézier et al., 2007).

Some modelling studies are available on olfactory transduction in vertebrates (Lamb and Pugh, 1992b; Lindeman, 2001; Suzuki et al., 2002; Rospars et al., 2003a; Dougherty et al., 2005; Reidl et al., 2006). In insects, models of the reactions involved in perireception (PBP and lymph enzymes) and reception in moth pheromone sensilla (Kaissling, 1998a; Kaissling, 1998b; Kaissling, 2001; Minor and Kaissling, 2003; Rospars et al., 2003b; Kaissling and Rospars, 2004) have been developed. However, no modelling study is yet available for post-receptor transduction events in insects. The present paper is an attempt to fill this gap. First, a simplified model of perireceptor, receptor, and post-receptor events is proposed. Second, this model is utilized to determine quantitatively the kinetics of activated proteins (receptors, G-proteins, and effector enzymes) in the dendritic membrane as a function of the concentration of pheromone in the air delivered to the sensillum. Third, the model output is discussed by comparing the time course of the calculated protein densities to the experimentally measured time course of the receptor potential (Zack, 1979; see also Dolzer et al., 2003).

Table 1
Reaction network describing the uptake, perireception, reception and early amplification in the moth pheromone receptor neuron, showing the reaction steps[a] and species formed[b]

Uptake[c]:	$L_{air} \xrightarrow{k_i} L$	(1)
Deactivation:	$L + N \underset{k_{-LN}}{\overset{k_{LN}}{\rightleftarrows}} NL \xrightarrow{k_o} P + N$	(2)
Activation:	$R + L \xrightarrow{k_1} RL \xrightarrow{k_2} R^*$	(3)
	$R^* + G \xrightarrow{e_{RG}} R^* + G^* + G_b$	(4)
	$G^* + E \xrightarrow{e_{GE}} E^*$	(5)
Inactivation:	$R^* \xrightarrow{k_{-2}} RL \xrightarrow{k_{-1}} R + L$	(6)
	$G^* \xrightarrow{k_{Ga}} G_r$	(7)
	$E^* \xrightarrow{k_{Ea}} E + G_r$	(8)
	$G_r + G_b \xrightarrow{e_G} G$	(9)

[a] Notations for rate constants: see Table 2.

[b] Notations for species: L≡main pheromone component, P≡deactivated pheromone, N≡deactivating enzyme, R≡pheromone receptor, $R^* \equiv RL^*$ activated pheromone receptor, $G \equiv G_{\alpha\text{-}\beta\gamma\text{-}GDP}$, $G \equiv G^*_{\alpha\text{-}GTP}$, $G_b \equiv G_{\beta\gamma}$, $G_r \equiv G_{\alpha\text{-}GDP}$, E≡effector enzyme (phospholipase C), $E^* \equiv G^*_{\alpha\text{-}GTP}$ E. The reaction network involves 14 species: 3 for the pheromone (L_{air}, L, P), 2 for interactions $N \leftrightarrows L$ (N, NL), 3 for interactions $R \leftrightarrows L$ (R, RL, R^*), 4 for interactions $G \leftrightarrows R^*$ (G, G^*, G_b, G_r) and 2 for interactions $G \leftrightarrows E$ (E, E^*). Its description requires 12 ordinary differential equations (see Appendix A).

[c] Translocation reaction for pheromone entering the sensillar lymph from the surrounding air.

2. Model of the cascade

The reactions involved are shown in Table 1. The model studied involves 16 parameter values of two types, rate constants, and initial densities (Table 2). The perireceptor reactions take place in the lymph volume (in 3D) whereas the reactions involving receptor, G- and effector proteins take place within the membrane (in 2D). The model describing the fate of the pheromone molecules in the sensillum lymph is simplified since it considers only fast pheromone deactivation (hypothetical enzyme N, Kaissling, 2001) but no PBP. This simplification has no effect on the kinetics of activated receptors (Kaissling and Rospars, 2004). The parameter values for the perireceptor reactions and the pheromone-receptor interactions were estimated initially by Kaissling (2001) and Minor and Kaissling (2003).

The reaction rates between membrane proteins (receptors, G-proteins, and effectors) are presently unknown in the ORN. Their encounters depend on their

Table 2
Values of parameters used in numerical simulations of the neuron type sensitive to the main pheromone component[a]

Protein concentrations[a]		
$N_0 = 3700$	molec μm^{-2}	Kaissling (2001); Kaissling and Rospars (2004); 1 μM
$R_0 = 6000$	molec μm^{-2}	Kaissling (2001); Kaissling and Rospars (2004); 1.64 μM
$G_0 = 1000$	molec μm^{-2}	This paper
$E_0 = 500$	molec μm^{-2}	This paper
Reaction rate constants[b]		
$k_i = 2.9 \times 10^4$	s^{-1}	Kaissling (pers. com.), Rospars et al. (2003b)
$k_o = 30$	s^{-1}	Kaissling (2001); Kaissling and Rospars (2004)
$k_{LN} = 1.1 \times 10^{-3}$	s^{-1} molec^{-1} μm^2	Kaissling (2001); Kaissling and Rospars (2004); 4 $\mu M^{-1}.s^{-1}$
$k_{-LN} = 100$	s^{-1}	Kaissling (2001); Kaissling and Rospars (2004)
$k_1 = 5.6 \times 10^{-5}$	s^{-1} molec^{-1} μm^2	Kaissling (2001); 0.2 $\mu M^{-1}.s^{-1}$), Sakurai et al., 2004(2004; $k_{-1}/k_1 \approx 40$ μM)
$k_{-1} = 8$	s^{-1}	Minor and Kaissling (2003)
$k_2 = 17$	s^{-1}	Minor and Kaissling (2003)
$k_{-2} = 100$	s^{-1}	Minor and Kaissling (2003)
$k_{Ga} = 0.05$	s^{-1}	Antonny et al. (1993); Felber et al. (1996)
$k_{Ea} = 2$[c]	s^{-1}	Vuong and Chabre (1991); Felber et al. (1996)
Reaction rate constants limited by diffusion		
$e_{RG} = 0.75$[c]	$\mu m^2\ s^{-1}$	Lamb and Pugh (1992a); Felber et al. (1996)
$e_G = 2$	$\mu m^2\ s^{-1}$	Hofmann and Heck (1996); Felber et al. (1996)
$e_{GE} = 0.3$	$\mu m^2\ s^{-1}$	Lamb and Pugh (1992a); Felber et al. (1996)

[a] Concentration of N in lymph (in μM) was converted to an equivalent density on membrane with $V = 2600\ \mu m^3$ (volume of the hair) and $S = 426\ \mu m^2$ (surface of outer dendrite) (from Keil, 1984). The conversion factor from uM to molec/μm^2 is $N_A \times (V/S) \times 10^{-21}$, with N_A Avogadro's number.
[b] Similarly, the rate constants of the bimolecular reactions (k_{LN} and k_1 in $\mu M^{-1}\ s^{-1}$) were converted to s^{-1} molec^{-1} μm^2.
[c] Modified values $k_{Ea} = 20\ s^{-1}$ and $e_{RG} = 0.15\ \mu m^2\ s^{-1}$ were also tested.

lateral diffusion in the membrane and, thus, depend on their sizes. Their diffusion-limited rate constants (e_{RG}, e_{GE}, e_G), as well as the decomposition reactions of the activated G-proteins (k_{Ga}) and activated effectors (k_{Ea}), can be tentatively derived from the corresponding reactions in the vertebrate rod photoreceptor (see references in Table 2). For the densities (molecules μm^{-2}) of G-proteins (G_0) and effector enzymes (E_0), which are also unknown, the proposed values are conjectures.

The standard set of reaction rates (Table 2) was derived from these assumptions. In order to account for experimental data, we examined also a different set with two modified rates (see Table 2, note c). These modifications concern the activation of G-proteins by receptors (e_{RG}), which is slower than in the photoreceptor, and the decomposition of the actived effector (k_{Ea}), which is faster than in the photoreceptor.

The reactions were expressed as a set of ordinary differential equations (see Appendix A). This means that all calculations were done assuming a relatively large number of molecules of each species, ignoring stochastic fluctuations, spatial effects and time-variation of the diffusion-limited rates.

The reaction system was subjected to pheromone square impulse of constant duration (2 s) and variable height (stimulus intensity). As shown by Kaissling (1998a), the intensity of stimulation is best expressed as a pheromone uptake, that is "the number of pheromone molecules adsorbed per unit volume of the perireceptor compartment and per unit time". In practice we expressed this uptake U in $\mu M\ s^{-1}$. Both volume and surface reactions being involved, concentrations and densities were all converted in molecules μm^{-2} for calculations (see Table 2).

3. Results

Given the initial concentrations, the reaction rates (Table 2) and the system of ordinary differential equations (in Appendix A) representing the reaction scheme of Table 1, the time courses of all species concentrations shown in Table 1 can be computed at any time for any given stimulation. These calculations were done for the same stimulation conditions as used by Zack (1979) (see also Kaissling, 2001) in her experiments. For the sake of simplicity, in the present account, we consider only the activated form of the receptors and effector enzymes.

3.1. Time course of the response (Fig. 1)

With single pulses of 2 s duration and various uptakes, expressed in μM of pheromone per second entering the

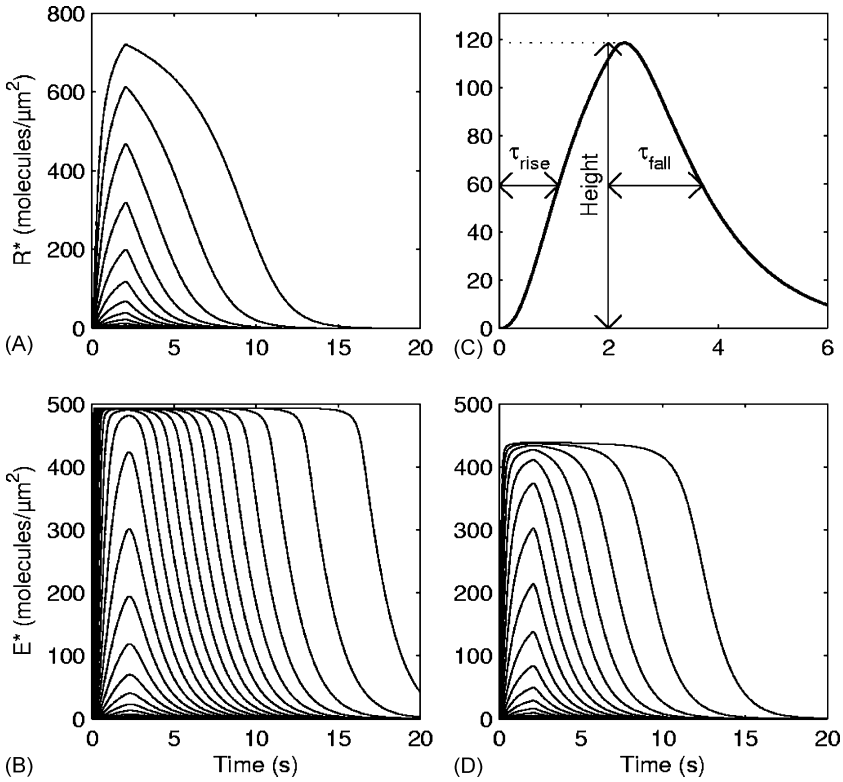

Fig. 1. Time courses of the activated receptors R^* (A) and activated effectors E^* (phospholipase C, B, D) in response to 2-s square pulses. Responses are shown for pulses yielding various uptakes, regularly spaced by 0.25 log units from 10^{-5} to 10^{2} μM/s (29 pulses), for the standard parameter values (A, B) and the modified values of k_{GE} and e_{RG} (D, see Table 2, note c). (C) Definition of the response characteristics: height, half-rise time τ_{rise}, and half-fall time τ_{fall}.

sensillum, the calculated densities of all activated proteins rise from zero at stimulus onset, reach a maximum (e.g. E^*_{peak}), then return to zero after stimulus offset, like the receptor potential. Starting from the lowest intensity of the stimulation, the height of the response increases with the stimulus intensity. However, beyond a certain intensity, the shape of the E^* responses is no longer a sharp peak but presents a plateau. Thus, the system shows two qualitatively distinct regimes, one where the height varies and the other where it remains constant while the duration increases. The duration of the plateau is longer for the standard values of the parameters (Fig. 1B) than for the modified values of e_{RG} and k_{Ea} (Fig. 1D). A more quantitative description can be achieved using the height, half-rise time, and the half-fall time of the responses at different intensities, as explained now.

3.2. Heights

The heights R^*_{peak} and E^*_{peak} of the responses increase with the stimulus uptake U. As shown in Fig. 2A and D, these are sigmoid curves in semilog scale, which increase from zero at low uptake to maximum values at high uptake. At the peak, whereas 88% or more of the effectors are activated (total density E_0 being 100%), only 12% of receptors are activated. These curves can be characterized by their rising point, saturation point, and dynamic range.

Taking the asymptotic maxima as references, the sigmoid curves can be characterized by the uptakes at which 1% (rising) and 99% (saturation) of proteins are activated. With the standard values of the parameters the corresponding uptakes are $10^{-0.25}$ (1%) and 100 μM s^{-1} (99%) for R^*, 10^{-3} and $10^{-0.5}$ μM s^{-1} for E^* (Fig. 2A). The dynamic ranges, which are the ratios expresssed in log units of the uptakes at saturation and at rising, are ca. 1.75 and 2.5 log units respectively, indicating that both curves are steep and almost parallel. The shift of the 1% point towards smaller uptakes along the transduction cascades, shows that the initial R^* response is about 500 times less sensitive than the E^* response. With the modified parameters (e_{RG} and k_{Ea}) the range becomes $10^{-1.5}$

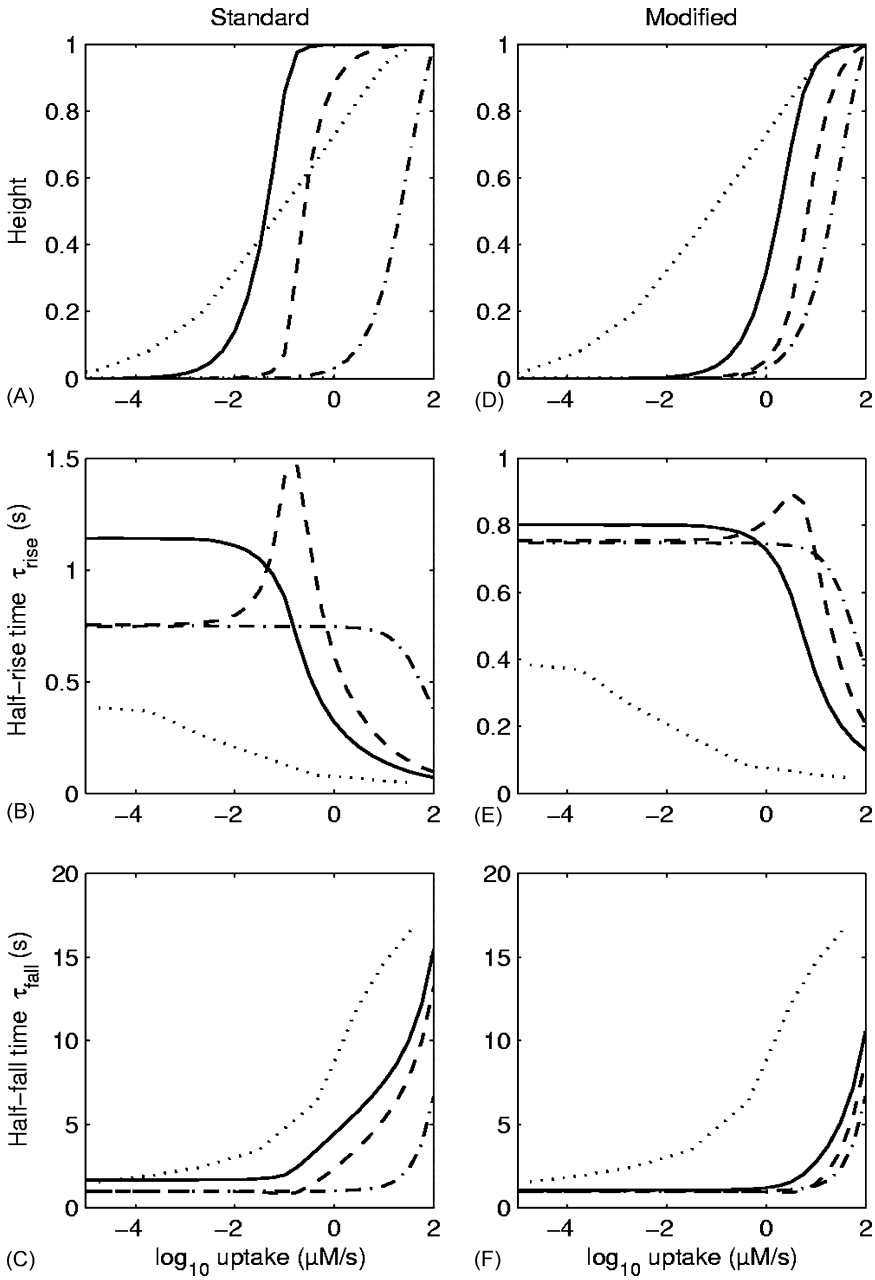

Fig. 2. Response characteristics of activated proteins R^* (dash-dot), G^* (dash), E^* (solid) and experimentally observed receptor potential V (dot) as a function of stimulus uptake. The characteristics are defined in Fig. 1C. Relative heights (A, D), half-rise times τ_{rise} (B, E), and half-fall times τ_{fall} (C, F) shown for the standard values of the parameters (left column) and the modified values of e_{RG} and k_{Ea} (right column; see Table 2, note c). In A (respect. D), the relative heights $X_r = X/\max(X)$ where maximum heights, $\max(X)$, are 720 R^*, 504 (respect. 475) G^*, 493 (respect. 438) E^* molec/µm^2 and 30 mV (V). V data by courtesy of K.-E. Kaissling (see Zack, 1979 and Kaissling, 2001).

to $10^{1.75}$ µM s^{-1} for E^*, so that the increase in sensitivity is much smaller (18 times); the E^* curve remains close to the R^* curve (Fig. 2D). Although the dynamic range of E^* widens by 0.25 log units, it extends on only a fraction of the ca. 7.5 range found experimentally for the receptor potential.

3.3. Half-rise and half-fall times

The time needed by the activated proteins to reach their peak value depends on the stimulus uptake. However, the activated molecules tend asymptotically to the steady state, so that a precise time to peak is difficult to

define. For this reason, in accordance with experimental measurements, we preferred to use the half-rise time, which is the time elapsed between stimulation onset and 50% of the maximum response (Fig. 1C). In this part of the temporal response the slope of the curve is relatively steep, so that the half-rise time is always well defined. A similar approach was followed to analyze the decline of the responses, the half-fall time being defined as the time elapsed between stimulus offset and the decline of the response to 50% of its maximum value (Fig. 1C).

The calculated half-rise and half-fall times of the activated proteins present the same global behavior. At low uptakes they are constant (or slowly changing), then beyond a certain point they respectively decrease (Fig. 2B and E) or increase (Fig. 2C and F). The transitions take place close to the uptake yielding the half-maximum peak response so that the range of uptakes for which times are constant is wider for R^* than for E^* and with the modified constants than with the standard ones. Interestingly the times for E^* are practically equal to those for R^* in this constant part with the modified constants. At most uptakes the calculated times are either greater (rising time) or smaller (falling time) than those measured on the receptor potential, the difference being smaller at high uptake for rise and at low uptake for fall.

4. Discussion

4.1. Modelling olfactory transduction

Although much experimental work has been devoted to investigating the various properties of pheromone reception in moths, no complete model has yet been proposed to account quantitatively for these properties. Building upon the pioneering modelling work of Kaissling et al. on the perireceptor and receptor events (Kaissling, 1998a,b; Kaissling, 2001; Minor and Kaissling, 2003), we have concentrated on the post-receptor events. These events involve the interactions of receptor, G-protein, and phospholipase C molecules within the dendritic membrane. In the model studied, the G-protein cascade obeys the concept of the random walk amplifier (Liebman and Pugh, 1979) in which the proteins freely diffuse on the two-dimensional dendritic membrane, so that each activated receptor can sequentially encounter and activate several molecules of G-protein. Then, each of the active G-protein molecules can in turn bind and activate an effector molecule. In this model, the reactions are limited by diffusion, not by direct interaction of the partners. The responses are turned off by deactivation reactions acting on the receptor, the G-protein, and the effector.

4.2. Limitations

Before interpreting the results obtained it must be pointed out that they are subject to four kinds of limitations.

The first one comes from the uncertainties on the numerical parameters. Values based either on direct experimental measurements in moth pheromone ORNs or derived from models integrating such measurements, were used when available. However, to our knowledge, no values were estimated for the densities and reaction rates of the G-protein and the effector in the ORN. The diffusion-limited rate for the G-protein transducin and the phosphodiesterase effector in the rod photoreceptor (Lamb and Pugh, 1992a; Felber et al., 1996) were used as replacements. It is expected that their properties are similar in both the photoreceptor neuron and the ORN. However, there is no reason to believe that either the densities or even the ratios of the proteins are the same in both neuron types and therefore the densities we have chosen for these proteins are conjectural. Also, the activation of a G-protein when reacting with an activated receptor (controlled by rate constant e_{RG}) and the deactivation of the activated effector (controlled by rate constant k_{Ea}) might differ in the ORN. For this reason we studied modified values of the latter two parameters.

The second limitation comes from the fact that the model studied is described by a set of ordinary differential equations (ODEs). This means that the numbers of molecules involved must be large enough to be considered as continuous variables. This condition is met for uptakes greater than ca. $10^{-2.5}$ $\mu M\,s^{-1}$ when the number of activated molecules R^* per ORN exceeds 30. In the present ODE model the uptake which yields a single R^* per ORN is 10^{-4} $\mu M\,s^{-1}$. Kaissling and Priesner (1970) showed that, at the behavioral threshold ca. 10^{-6} $\mu M\,s^{-1}$, a single receptor per ORN is activated and can trigger a spike. Preliminary numerical experiments indicate that such a low threshold will be obtained using a stochastic approach (which is valid for a single R^*).

A third limitation comes from the uncertainties on the exact mechanism of pheromone deactivation in the perireceptor space. The deactivating enzyme N considered here is hypothetical and was postulated by Kaissling (1972) because the pheromone adsorbed on the antenna has a much longer half-life than the cell response. Its action is dynamically equivalent to the more complex perireception system proposed by Kaissling (2001), both systems yielding exactly the same kinetics of activated receptors.

The fourth limitation arises from the fact that the most precise data currently available on transduction

result from the measurement of the receptor potential, whereas the present model does not take into account the post-effector steps, that is the second messenger and the various channels (including calcium channels), that are involved in its generation. Thus, assuming the parameter values of the present model are well chosen, any difference in height and temporal properties between the effector response and the receptor potential must be explained by these post-effector steps.

4.3. Small amplification factor and small delays in the RGE cascade

If the constants describing the perireceptor and receptor events are essentially correct, then the reaction rates describing the post-receptor events in the photoreceptor cannot apply to the ORN. The main reason for this conclusion comes from the height of the effector response as a function of pheromone uptake (Figs. 1B) and its comparison to the corresponding curve measured on the receptor potential (Fig. 2A). The two curves expressed in relative values, E_r^* and V_r (see legend of Fig. 2) cross one another and although they reach half-maximal response at the same uptake (ca. $10^{-1.5}\,\mu M\,s^{-1}$), they have significantly different rising points, saturations points, and dynamic ranges (i.e. slopes). To account for these differences we would have to postulate that the amplification factor V_r/E_r^* of the post-effector steps is larger than 1 up to $10^{-1.5}\,\mu M\,s^{-1}$ and smaller than 1 beyond, which seems difficult to explain.

Decreasing e_{RG} five times and increasing k_{Ea} ten times with respect to their values in the photoreceptor, slows down the activation of G-proteins and accelerates the deactivation of effectors, resulting in two significant effects:

First, the amplification factor E^*/R^* of the cascade falls from 330 to 7.5 (Fig. 2A and D). Consequently the effector curve is shifted towards high uptakes and saturates close to the uptake at which the receptor potential V saturates, so that the E_r^* and V_r curves no longer cross. Now the amplification factor V_r/E_r^* of the post-effector steps is always greater than 1 for all uptakes, although it varies, being maximum at small uptakes then progressively tending to one at high uptake. The small value of the amplification factor found (7.5) is in agreement with the recent finding by Takeuchi and Kurahashi (2005) that the second-messenger (cAMP) production in the frog ORN cilia is extremely small with respect to cGMP hydrolysis in the rod photoreceptor.

Second, the rise (Fig. 2B and E) and fall (Fig. 2C and F) times of E^* become very similar to those of R^*, especially at low uptake. Although E^* follows causally R^*, so that its transients must be delayed and proceed more slowly, this slowing down is very small (rise) or negligible (fall). Therefore, the production and removal of G^* and E^* must be much faster than those of R^*. This interpretation is in agreement with Kaissling's (2001) conclusion that post-receptor processes must be fast enough to follow quickly any change of R^* upon a change of stimulus intensity.

4.4. Role of the post-effector steps

If the differences between the model output and the receptor-potential measurements result from the post-effector steps, several consequences follow. The first one is that these steps can significantly increase the dynamic range of the response, which means that the 1% rising point of the electrical response is much lower than that of the effector. As a consequence, most of the amplification in the cascade is expected to arise from the second messenger(s) and the ionic channels. Secondly, the electrical response rises faster than the effector response, so decreasing the half-rise time. This effect may seem paradoxical but can result from the amplification factor just mentioned. Thirdly, possibly for the same reason, the electrical response falls more slowly than the effector response suggesting a significant contribution of the post-effector steps to the decline of the receptor potential.

Acknowledgements

The authors thank Janos Toth for helpful discussions, Karl-Ernst Kaissling for critical comments on successive versions of this paper, and Christine Young for linguistic corrections. This work was supported by ANR Aromalim (05-PNRA-002).

Appendix A. System of differential equations

$$U = k_i L_{air} \tag{A1}$$

$$\frac{dL}{dt} = U - k_{LN} L \cdot N + k_{-LN}(LN) - k_a R \cdot L + k_{-a}(RL) \tag{A2}$$

$$\frac{d(LN)}{dt} = -k_{LN} L \cdot N - (k_{-LN} + k_o)(LN) \tag{A3}$$

$$\frac{dN}{dt} = -k_{LN} L \cdot N - (k_{-LN} + k_o)(LN) \tag{A4}$$

$$\frac{dR}{dt} = -k_1 R \cdot L + k_{-1}(RL) \tag{A5}$$

$$\frac{d(RL)}{dt} = k_1 R \cdot L - (k_2 + k_{-1})(RL) + k_{-2} R^* \quad \text{(A6)}$$

$$\frac{dR^*}{dt} = k_2(RL) - k_{-2} R^* \quad \text{(A7)}$$

$$\frac{dG}{dt} = -e_{RG} R^* \cdot G + e_G G_r G_b \quad \text{(A8)}$$

$$\frac{dG^*}{dt} = e_{RG} R^* \cdot G - e_{GE} G^* \cdot E - k_{Ga} G_a^* \quad \text{(A9)}$$

$$\frac{dG_b}{dt} = e_{RG} R^* \cdot G - e_G G_r \cdot G_b \quad \text{(A10)}$$

$$\frac{dG_r}{dt} = k_{GA} G^* + k_{GE} E^* - e_G G_r \cdot G_b \quad \text{(All)}$$

$$\frac{dE}{dt} = -e_{GE} G^* \cdot E + k_{GE} E^* \quad \text{(A12)}$$

$$\frac{dE^*}{dt} = -e_{GE} G^* \cdot E - k_{GE} E^* \quad \text{(A13)}$$

References

Antonny, B., Otto-Bruc, A., Chabre, M., Vuong, T.M, 1993. GTP hydrolysis by purified subunit of transducin and its complex with the cyclic GMP phosphodiesterase inhibitor. Biochemistry 32, 8646–8653.

Breer, H., Boekhoff, I., Tareilus, 1990. Rapid kinetics of second messenger formation in olfactory transduction. Nature 345, 65–68.

Buck, L., Axel, R., 1991. A novel multigene family may encode odorant receptors: a molecular basis for odor recognition. Cell 65, 175–187.

Dolzer, J., Fisher, K., Stengl, M, 2003. Adaptation in pheromone-sensitive trichoid sensilla of the hawkmoth *Manduca sexta*. J. Exp. Biol. 206, 1575–1588.

Dougherty, D.P., Wright, G.A., Yew, A.C., 2005. Computational model of the cAMP-mediated sensory response and calcium-dependent adaptation in vertebrate olfactory receptor neurons. Proc. Natl. Acad. Sci. U.S.A. 102, 10415–10420.

Felber, S., Breuer, H.P., Petruccione, F., Honerkamp, J., Hofmann KP, 1996. Stochastic stimulation of the transducin GTPase cycle. Biophys. J. 71, 3051–3063.

Hofmann, K.P., Heck, M., 1996. Light-induced protein-protein interactions on the rod photoreceptor disc membrane. Biomembranes 2, 1–100.

Ishida, Y., Leal, W.S., 2005. Rapid inactivation of a moth pheromone. Proc. Nat. Acad. Sci. U.S.A. 102, 14075–14079.

Jacquin-Joly, E., Merlin, C., 2004. Insect olfactory receptors: contribution of molecular biology to chemical ecology. J. Chem. Ecol. 30, 2359–2397.

Kaissling, K.-E., 1972. Kinetic studies of transduction in olfactory receptors of *Bombyx mori*. In: Schneider, D. (Ed.), Int. Symp. Olf. Taste IV. Wissensch Verlagsgesellsch, Stuttgart, pp. 207–213.

Kaissling, K.-E., 1998a. Flux detectors versus concentration detectors: two types of chemoreceptors. Chem. Senses 23, 99–111.

Kaissling, K.-E., 1998b. Pheromone deactivation catalyzed by receptor molecules: a quantitative kinetic model. Chem. Senses 23, 385–395.

Kaissling, K.-E., 2001. Olfactory perireceptor and receptor events in moths: a kinetic model. Chem. Senses 26, 125–150.

Kaissling, K.-E., 2004. Physiology of pheromone reception in insects (an example of moths). Anir 6, 73–91.

Kaissling, K.-E., Priesner, E., 1970. Die riechschwelle des seidenspinners. Naturwiss. 57, 23–28.

Kaissling, K.-E., Rospars, J.-P., 2004. Dose-response relationships in an olfactory flux detector model revisited. Chem. Senses 29, 529–531 (Erratum 29: 747).

Kasang, G, 1971. Bombykol reception and metabolism on the antennae of the silkmoth *Bombyx mori*. In: Ohloff, G., Thomas, A.F. (Eds.), Gustation and Olfaction. Academic Press, London, pp. 245–250.

Keil, T.A., 1984. Reconstruction and morphometry of silkmoth olfactory hairs: a comparative study of sensilla trichodea on the antennae of male *Antheraea polyphemus* and *Antheraea pernyi* (Insecta Lepidoptera). Zoomorphology 104, 147–156.

Krieger, J., Grosse-Wilde, E., Gohl, T., Dewer, Y.M., Raming, K., Breer, H., 2004. Genes encoding candidate pheromone receptors in a moth (*Heliothis virescens*). Proc. Natl. Acad. Sci. U.S.A. 101, 11845–11850.

Lamb, T.D., Pugh, E.N., 1992a. A quantitative account of the activation steps involved in phototransduction in amphibian photoreceptors. J. Physiol. 449, 719–758.

Lamb, T.D., Pugh, E.N., 1992b. G-protein cascades: gain and kinetics. Trends Neurosci. 15, 291–298.

Liebman, P.A., Pugh Jr., E.N., 1979. The control of phosphodiesterase in rod disk membranes: kinetics, possible mechanisms and significance for vision. Vision Res. 19, 375–380.

Lindeman, B., 2001. Predicted profile of ion concentrations in olfactory cilia in the steady-state. Biophys. J. 80, 1712–1721.

Maida, R., Redkozubov, A., Ziegelberger, G., 2000. Identification of PLC beta and PKC in pheromone receptor neurons of *Antheraea polyphemus*. NeuroReport 11, 1773–1776.

Minor, A.V., Kaissling, K.-E., 2003. Cell responses to single pheromone molecules may reflect the activation kinetics of olfactory receptor molecules. J. Comp. Physiol. A 189, 221–230.

Nakagawa, T., Sakurai, T., Nishioka, T., Touhara, K., 2005. Insect sex-pheromone signals mediated by specific combinations of olfactory receptors. Science 307, 1638–1641.

Pézier, A., Rospars, J.-P., Lucas, P., 2007. Ca^{2+} stabilizes the membrane potential of moth olfactory receptor neurons at rest and is essential for their fast repolarization, Chemical Senses, submitted for publication.

Pophof, B., van der Goes van Nanters, W.M., 2002. Activation and inhibition of the transduction process in silkmoth olfactory receptor neurons. Chem. Senses 27, 435–443.

Reidl, J., Borowski, P., Sensse, A., Starke, J., Zapotocky, M., Eiswirth, M., 2006. Model of calcium oscillations due to negative feedback in olfactory cilia. Biophys. J. 90, 1147–1155.

Rospars, J.-P., Lansky, P., Duchamp-Viret, P., Duchamp, A., 2003a. Relation between stimulus and response in frog olfactory receptor neurons in vivo. Eur. J. Neurosci. 18, 1135–1154.

Rospars, J.-P., Lansky, P., Krivan, V., 2003b. Extracellular transduction events under pulsed stimulation in moth olfactory sensilla. Chem. Senses 28, 509–522.

Sakurai, T., Nakagawa, T., Mitsuno, H., Mori, H., Endo, Y., Tanoue, S., Yasukochi, Y., Touhara, K., Nishioka, T., 2004. Identification and functional characterization of a sex pheromone receptor in the silkmoth *Bombyx mori*. Proc. Natl. Acad. Sci. U.S.A. 101, 16653–16658.

Stengl, M., 1994. Inositol-triphosphate-dependent calcium currents precede cation currents in insect olfactory receptor neurons in vitro. J. Comp. Physiol. A 174, 187–194.

Stengl, M., Ziegelberger, G., Boekhoff, I., Krieger, J., 1999. Perireceptor events and transduction mechanisms in insect olfaction. In: Hansson, B.S. (Ed.), Insect Olfaction. Springer, Berlin Heidelberg New York, pp. 49–66.

Suzuki, N., Takahata, M., Sato, K., 2002. Oscillatory current responses of olfactory receptor neurons to odorants and computer simulation based on a cyclic AMP transduction model. Chem. Senses 27, 789–801.

Takeuchi, H., Kurahashi, T., 2005. Mechanism of signal amplification in the olfactory sensory cilia. J. Neurosci. 25, 11084–11091.

Vogt, R.G., 2004. Molecular basis of pheromone detection in insects. In: Gilbert, L.I., Iatro, K., Gill, S. (Eds.), Comprehensive Insect Physiology, Biochemistry, Pharmacology and Molecular Biology. Elsevier.

Vuong, T.M., Chabre, M., 1991. Deactivation kinetics of the transduction cascade of vision. Proc. Natl. Acad. Sci. U.S.A. 88, 9813–9817.

Zack, C., 1979. Sensory adaptation in the sex pheromone receptor cells of Saturniid moths. PhD Thesis. Ludwig-Maximilians-Universität, Munich, 99 pp.

Zufall, F., Hatt, H., 1991. Dual activation of a sex-dependent ion channel from insect olfactory dendrites by protein kinase C activators and cyclic GMP. Proc. Natl. Acad. Sci. U.S.A. 88, 8520–8524.